Nanotechnology for Environmental Engineering (2020) 5:6
https://doi.org/10.1007/s41204-020-0068-0

ORIGINAL PAPER

# Kinetics and thermodynamics of textile dye removal by adsorption onto iron oxide nanoparticles

**Arzu Yakar[1] · Ahmet Ünlü[2] · Tolga Yeşilçayır[2] · İbrahim Bıyık[2]**

Received: 17 September 2019 / Accepted: 20 January 2020 / Published online: 5 February 2020


## Abstract

Contamination of potable water supplies will in the future lead to the emergence of problems like lack of water. Therefore, the issues such as environmental pollution and the purification of water have been a major focus of scientists recently. Especially, the removal of the heavy metals and organic substances that are harmful to human health and exist in industrial waste water is of great importance. In this study, removal of textile dye (Maxilon® Blue GRL 300%, MBG), which is a significant impurity, from water was carried out by using iron oxide nanoparticles. Iron oxide nanoparticles were synthesized by using co-precipitation method. XRD, SEM, TEM, size distribution, zeta potential and magnetic properties measurements were performed to investigate the properties of the nanoparticles. The MBG removal capacities of iron oxide nanoparticles were investigated by taking into account the initial metal ion concentration, pH of aqueous medium, time and temperature. The dye adsorption capacity of iron oxide nanoparticles increased with an increase in dye concentration and temperature. The highest dye removal was observed at pH 9.0. According to the evaluation of the dye concentration effect on adsorption process, when the highest concentration of 25.0 mg/L dye solution was used at room temperature, the highest dye adsorption capacity was determined as 0.23 mg/g. The results of adsorption kinetics and thermodynamic data have shown that adsorption process has pseudo-second-order kinetics and endothermic form. Adsorption studies data have well fitted to Langmuir isotherm at room temperature.

**Keywords** Magnetite · Characterization · Maxilon blue GRL · Adsorption · Waste water treatment · Iron oxide nanoparticles

## Introduction

Today, water is one of the most important natural resources. While 97.5% of the water in the Earth is saline, the remaining 2.5% water belongs to the freshwater resources. However, 68.7% of freshwater resources is still trapped in the ice. The remaining 30% is situated underground. Fresh surface water sources such as rivers and lakes hold a smaller rate than 1% of the total water in the world. Increasing world population, irregular urbanization, rapid industrialization and climate change are reducing the number of clean and potable water each passing day.

Pollution of potable water resources will cause problems such as lack of water in the future. Therefore, countries, organizations and unions have encouraged scientists to work on important issues such as environmental pollution removal and water treatment. Especially, in the treatment of waste water, the removal of heavy metals and organic substances being harmful to human health is of great importance [19, 26, 29, 44]. Due to the colored waters adversely affect living organisms, the national and international importance of carrying out color control in the industrial waste water that is discharged into the receiving environment is increasing every day. Discharging the color waste water into the receiving environment directly reduces the light transmittance of water and the amount of dissolved oxygen in the medium. In addition to that, colorants as well as partitioning products have toxic and/or mutagenic effects on organisms. Therefore, color parameter takes also an important part in the water

✉ Arzu Yakar
ayakar@pau.edu.tr

[1] Department of Chemical Engineering, Faculty of Engineering, Pamukkale University, Denizli, Turkey

[2] Department of Chemical Engineering, Faculty of Engineering, Afyon Kocatepe University, Afyonkarahisar, Turkey

discharge criteria along with other pollutants such as suspended solids and dissolved organic solid matter. Colored waste water producing industries can be counted as textile, food, paper and metal. Among these industries, textile industry with its 92% is one that has the largest percentage because of using dye materials. Since the waste water of these textile firms has a wide variety of pollutants and the pollution load of waste water especially due to the dyeing is lot, it raises the necessity to use a combination of different methods for treating waste water from the textile industry.

Therefore, physical, chemical and biological methods are used altogether in various combinations in the plants. The methods that the textile companies prefer for the chemical treatment are as follows: coagulation–flocculation, chemical oxidation, neutralization and ozonation processes. However, most of the widely used biological treatment processes or some of the combined system are effective in the removal of COD and turbidity although they are very ineffective in color removal. On the condition that the textile wastewater is discharged into the freshwater resources before it reaches the desired discharge criteria, sunlight will not be able to penetrate into the water due to the presence of colorant materials in the water. The amount of dissolved oxygen in the water will decrease so that this will create an annoying factor to threaten aquatic life. Therefore, the purification of wastewater of textile industry is very important for the ecological life cycle.

In order to remove dyes from waste water, there are many studies on the use of adsorption process. For this purpose, it is observed that in these studies, active carbon, clay minerals, composite materials, organic wastes and polymers were commonly used as adsorbent materials [28, 34, 36, 38]. In the last decade, there has been a remarkable increase in researches on waste water treatment by using functional properties imparted nanoparticles or magnetic polymer-coated nanoparticles [8, 42]. Zhou et al. [47] prepared glutaraldehyde cross-linked magnetic chitosan nanoparticles (GMCNs) and used them in order to remove FD&C Blue 1 and D&C Yellow 5 food dyes from the aqueous solution. Song et al. [37] worked to remove methyl orange (MO), reactive brilliant red K-2BP (RBR) and Acid Red 18 (R), which are the anionic dyes, from the waste water by using amine/$Fe_3O_4$-resin. In addition, Ge et al. [13] prepared magnetic nanoparticles (MNPs) modified with 3-aminopropyltriethoxysilane and copolymers of acrylic acid and crotonic acid and used them to remove the cationic dyes—crystal violet, methylene blue and alkali blue 6B, which exist in aqueous environment. Li et al. [25] synthesized $Fe_3O_4$@chitosan@graphene oxide and used it to remove the methylene blue (MB) dye from the water.

Also, Yao et al. [43] prepared porous magnetic polyacrylamide microspheres and used these microspheres to remove MB, neutral red (NR) and gentian violet (GV) from water. Moreover, Gao et al. [12] synthesized magnetic polymer multi-walled carbon nanotube (MPM-WCNT) nanocomposite and used them in orange II, sunset yellow FCF and amaranth in the aqueous solution, which are anionic azo dyes, to determine the adsorption capacity. In order to minimize initial investment and operating costs in the waste water treatment plants and to determine the most appropriate treatment type, it is very important to do the preliminary work. Although a lot of researches have been made with many composite materials (e.g., iron oxide–polymer, iron oxide–carbon nanotubes, etc.) including iron oxide ($Fe_3O_4$), the number of studies done by using only iron oxide ($Fe_3O_4$) nanoparticles is quite limited [22, 27]. The price of iron oxide ($Fe_3O_4$) will be cheaper than the price of the iron oxide ($Fe_3O_4$)-containing composite. Also, because the particle size of the magnetic polymeric nanoparticles is greater than the particle size of the magnetite nanoparticles, it was thought that using nanoparticles with a smaller grain size will increase the surface area/volume ratio and increase the treatment efficiency. Unlike studies using polymer-coated magnetic nanoparticles, in this study, it was aimed to investigate the treatment capacities of bare magnetic iron oxide nanoparticles in the waste water treatment since it is considered to be cost-reducing effect.

## Materials and methods

### Materials

In the synthesis of iron oxide magnetic nanoparticles, iron (II) chloride tetrahydrate ($FeCl_2{\cdot}4H_2O$, Sigma-Aldrich, 99%), iron (III) chloride hexahydrate ($FeCl_3{\cdot}6H_2O$, Sigma-Aldrich, 97%) and 32% ammonia solution (Merck, extra pure) were used. In the adsorption operation, the dyestuff (Maxilon® Blue GRL 300%; MBG, Huntsman) that is used in the textile industry and available from suppliers was used (Fig. 1). To adjust the pH value of the solution, 0.1 M hydrochloric acid (HCl, Merck) and 0.1 M sodium hydroxide (NaOH, Merck) solutions were utilized.

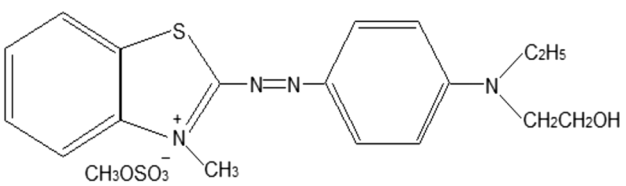


**Fig. 1** Chemical formula and structure of Maxilon® Blue GRL 300% (MBG) dye

## Method

### Synthesis of magnetic nanoparticles

In the synthesis of iron oxide nanoparticles, co-precipitation method was utilized [42]. In this method, $FeCl_2{\cdot}4H_2O$, $FeCl_3{\cdot}6H_2O$ salts and ammonia as precipitation agents were used. To prevent the oxidation of $Fe^{2+}$ and $Fe^{3+}$ salts and side reactions, synthesis operation was performed under nitrogen atmosphere. During synthesis, firstly 150 mL of aqueous solutions of $FeCl_3{\cdot}6H_2O$ and $FeCl_2{\cdot}4H_2O$ that fit the ratio of $Fe^{3+}/Fe^{2+}$ 2:1 was prepared and transferred to 5-necked glass flask. $N_2$ gas probe, temperature probe, reflux condenser and glass stirrer were placed, respectively, on the glass flask necks. After stirring the solution in the flask for 1 h with mechanical stirring at 85 ± 5 °C, 32% ammonia solution was added to the system. After adding ammonia solution, mixing was continued for another 30 min also. At the end of this process, the system was allowed to cool down to room temperature. The nanoparticles were removed from the solution using a magnet, and washing process was conducted with the distilled water until pH 9 is obtained. Upon completion of this procedure, sample was dried in a vacuum oven at 40 °C for one day. The reaction occurred during the synthesis is given below [23]:

$$Fe^{2+} + 2\,Fe^{3+} + 8\,OH^- \rightarrow Fe_3O_4 + 4\,H_2O$$

### Characterization

Structural characterization of the synthesized nanoparticles was determined through X-ray diffraction (XRD, Bruker D 8 Advance brand model). The morphology and particle size of all the synthesized nanoparticles were determined using scanning electron microscope (SEM, LEO 1430 VP model) and transmission electron microscope (TEM, FEI Tecnai G2 Spirit BioTwin model). MALVERN Nano ZS90 device was used to determine the size distribution of the synthesized particles.

The magnetic properties of nanoparticles were determined via vibrating sample magnetometer (Cryogenic Limited PPMS). After the adsorption, the surface elemental analysis of the particles was performed using the energy-dispersive X-ray (SEM/EDX, model LEO 1430 VP) device.

### Adsorption studies

In the adsorption experiments, synthesized iron oxide nanoparticles were used as adsorbent, while MBG was used as adsorbate. In the adsorption process, it was tried to determine the amount of adsorbent. For this purpose, varying amounts of adsorbent from 0.05 to 0.20 g were added to 25 mg/L of dye solution. After it has reached dye adsorption equilibrium value, the remaining dye concentration in the solution was measured via UV–Vis spectrophotometer (Shimadzu, UVmini 1240).

From the obtained data, adsorption capacity values were calculated ($q_e$) for each adsorbent material. In the adsorption kinetics study, the dye adsorption changes in time were investigated. In order to examine the effect of dye concentration on adsorption, 5 different dye solutions were used ranging from 5 to 25 mg/L. To study the effect of pH on adsorption, 3 different pH values (5, 7, 9) were used in the adsorption studies. Furthermore, studies were performed to examine the effect of temperature on the adsorption at 35 °C and 45 °C, except for room temperature. Adsorption capacity value of the magnetic particles is calculated using the following equation:

$$q_e = \frac{(C_i - C_e) \times V}{m} \tag{1}$$

where $C_0$ is the initial dye concentration (mg/L); $C_e$ is the dye concentration remaining in solution before adsorption at the equilibrium (mg/L); $V$ is the volume of the dye solution (L), and m is the mass of $Fe_3O_4$ nanoparticles in grams. In the kinetic calculations, $q_t$ was used instead of $q_e$ values, representing the adsorption capacity at time $t$.

## Results and discussion

### Characterization of magnetic nanoparticles

#### XRD analysis

Structural analysis of magnetic nanoparticles was performed by XRD analysis. Figure 2 shows the XRD pattern of magnetic nanoparticles.

As shown in Fig. 2, synthesized black striped pattern was determined belonging to the particles in compliance with iron oxide ($Fe_3O_4$) that is the red striped patterns of magnetite. It was understood later that the particles obtained at the end of the synthesis were the $Fe_3O_4$ in the crystalline structure. The average crystallite size was calculated by using the data obtained from the XRD analysis and the following Scherrer equation [31]:

$$L = \frac{K\lambda}{\beta\,\mathrm{Cos}\theta} \tag{2}$$

where $\lambda$ is the X-ray wavelength in nanometer (nm), $\beta$ is the peak width of the diffraction peak profile at half maximum height resulting from small crystallite size in radians, and $K$ is a constant related to crystallite shape, normally taken as

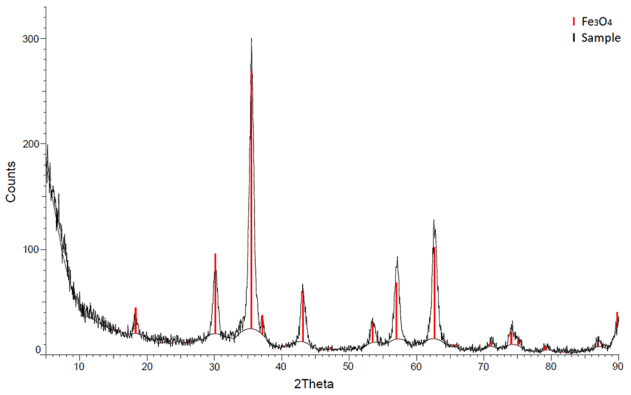


**Fig. 2** XRD pattern of the magnetic nanoparticles

0.9. The value of $\beta$ in $2\theta$ axis of diffraction profile must be in radians. The $\theta$ can be in degrees or radians, since the cos$\theta$ corresponds to the same number.

With the help of XRD analysis, the approximate crystal grain size of the particles was found to be 13.2 nm. Hariani et al. [17] carried out the synthesis using the co-precipitation method and obtained magnetite ($Fe_3O_4$) as a result of the XRD analysis. Wang et al. [40] have detected that the nanoparticles obtained by the co-precipitation method are the magnetite in the XRD analysis. And also, they have found out in their calculation using the data pattern of the Debye–Scherrer formula that the mean crystallite size of the samples is between 7 and 11 nm. They have determined that the particle size increased with increasing temperature and pH. Ghandoor et al. [14] have synthesized iron oxide nanoparticles by co-precipitation method in their study. They have noticed that the particles synthesized with $(NH_4)_2Fe(SO_4)_2$ and $FeCl_3$ are magnetite from XRD analysis. They also have calculated the value of average crystallite size as 10.0 nm by using the Scherrer equation.

### SEM and TEM analysis

The morphology of $Fe_3O_4$ magnetic nanoparticles synthesized using common precipitation method was investigated by SEM and TEM analysis. Figure 3 shows SEM and TEM images of $Fe_3O_4$ particles.

In the SEM images (Fig. 3) of $Fe_3O_4$ nanoparticles, it is seen that nano-size particles were obtained, but the particles were heavily agglomerated. On the other side, it was detected in the TEM images that the particles were agglomerated and one particle was in the size of 10–15 nm. In the study performed by Mascolo et al. [30], it was found out that in the SEM images of iron oxide particles that were obtained by the co-precipitation method, the particles were agglomerated. They have seen in the TEM images that the particles were in spherical shape and the grain size was about 11 nm. Shen et al. [35] have prepared differently shaped magnetite nanoparticles by using facile co-precipitation method in the presence of sodium dodecyl sulfate (SDS). They have determined that the obtained particles were agglomerated and their particle size went up to 15–50 nm with increasing SDS amount. All the synthesized iron oxide particles by the co-precipitation method have tended to be agglomerated in the water since they contain hydroxyl group [20].

### Particle size (DLS) and zeta potential analysis

The size distribution of $Fe_3O_4$ nanoparticles obtained was examined through the DLS analysis. The particle size distribution is shown in Fig. 4.

As it is seen from the particle size distribution graph that was obtained from DLS analysis, it is understood that the particles agglomerated (Fig. 4). These agglomerates can also be seen in the SEM and TEM analysis. Zeta potential value regarding the particles was found to be − 17.1 mV as a result of the analysis. The obtained experimental results illustrate also that the particles tend to come together by influencing each other depending on the electrical charge in the solution. This situation is favorable for helping nanoparticles to easily remove from waste water treatment systems.

### Magnetic saturation analysis

Magnetic saturation analysis was carried out via VSM device so as to determine the magnetic properties of the synthesized nanoparticles. The data gained from the analysis were transferred to graphics, and then, the hysteresis loop was created and is shown in Fig. 5.

As it is seen in Fig. 5, it was detected that the particles are superparamagnetic and the saturation magnetization (Ms) value is 66.50 emu/g. The saturation magnetization ($M_s$) of bare MNPs is 66.50 emu/g nanoparticles, which is less than that of bulk magnetite (90 emu/g). It was determined in the all previous studies in the literature that as the particle size decreases, Ms value decreases as well [5, 15, 16, 30, 45].

## Dye adsorption studies

### The effect of the amount of adsorbent on dye adsorption

To investigate the effects of nanoparticles amounts in the removal of MBG, which is a dye material, from aqueous solution, 4 different adsorbents amounts including 0.050 g, 0.10 g, 0.15 g and 0.20 g were used. The works were carried out in 25 mg/L initial MBG concentration at room temperature in 10 mL solution concentration. The effect of the amount of adsorbent on the adsorption capacity is shown in Fig. 6.

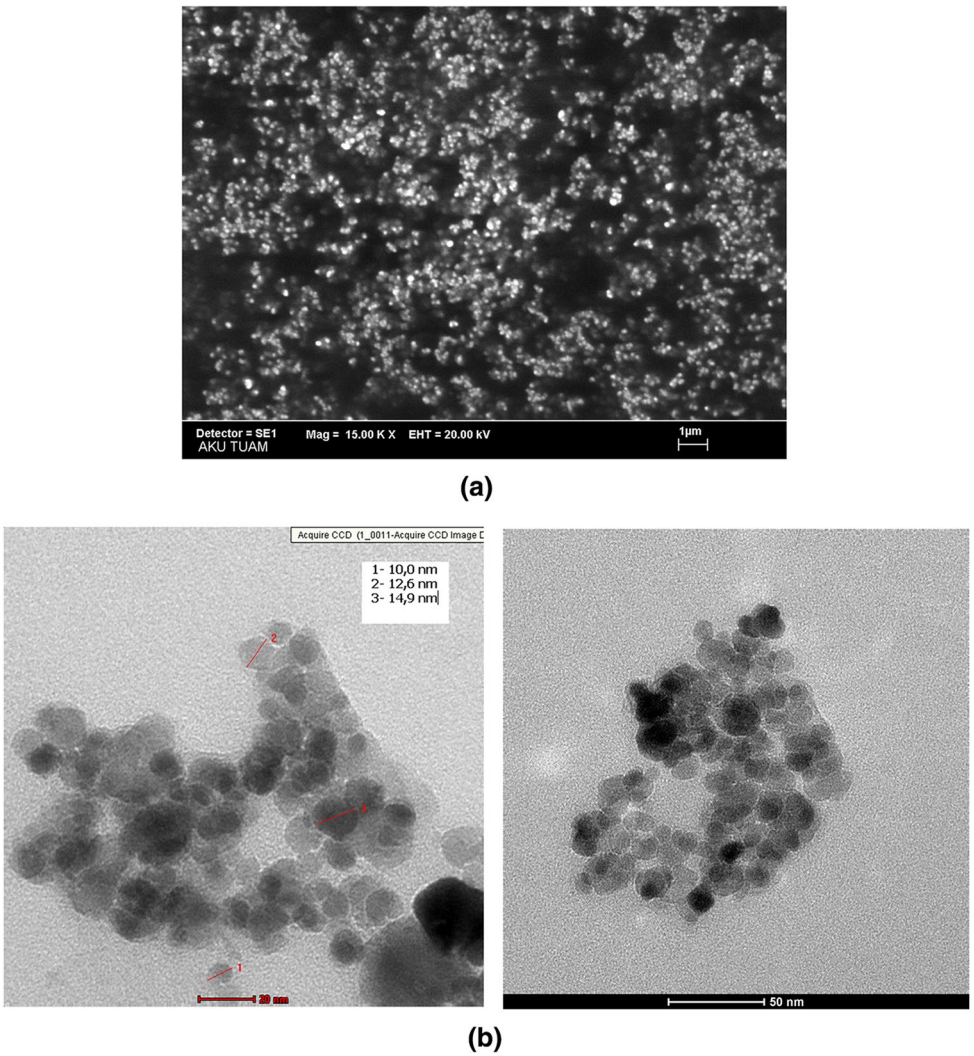


**Fig. 3** **a** SEM, **b** TEM images of magnetic nanoparticles

As seen from Fig. 6, when 0.050 g $Fe_3O_4$ was used, the highest adsorption capacity was gained as approximately 0.32 mg/g. At the end of the experiment, it was observed that there was an increase in the adsorbent value, while there was a decrease in the adsorption capacity. Due to the ease of weighing, 0.10 g of adsorbent quantity was used as a constant in all the experimental studies. Dye adsorption on $Fe_3O_4$ particles was supported with SEM–EDS analysis (Fig. 7).

As seen in Fig. 7, the peaks that belonged to Fe and O elements were detected on the surface of the adsorbent material along with N and C elements that belonged to dye molecules. SEM–EDS analysis shows that the adsorption has occurred.

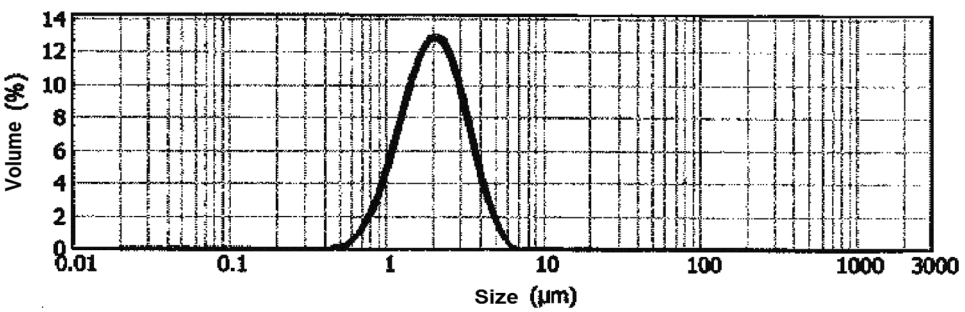


**Fig. 4** The distribution of particle size of magnetic nanoparticles

### Effect of initial dye concentration on dye adsorption

The graph obtained from the experiments that were performed with dye solution varying in 5–25 mg/L concentration is given in Fig. 8.

It was observed among the studies that there was an increase—albeit less—with the increasing initial dye concentration until 25 mg/L concentration of the adsorption capacity. On the other side, it was noticed in the 25 mg/L dye concentration that adsorption increases quite fast. Since the adsorbent material is nano-sized and leads to an increase in the mass/volume ratio, saturation could not be achieved at the highest concentration in terms of dye adsorption. The initial concentration provides an important driving force to overcome all mass transfer resistances of all molecules between the aqueous and solid phases [4, 9, 10, 18, 21].

The adsorption of dye on nanoparticles was analyzed by using Langmuir [24], Freundlich [11] and Temkin and Pyzhev [39] isotherms.

The linear form of Langmuir equation is given by Eq. 3 where $K_L$ is the Langmuir adsorption constant and $q_{max}$ is the adsorption capacity (mg/g):

$$\frac{C_e}{q_e} = \frac{C_e}{q_{max}} + \frac{1}{K_L \cdot q_{max}} \tag{3}$$

Calculated parameters using Eq. 3 are given in Table 1, and $K_L$ and $q_{max}$ constants were evaluated from the slope and the intercept of the linear plots of $C_e/q_e$ versus $C_e$, respectively.

The Langmuir isotherm is developed to explain monolayer coverage of adsorbate molecules on adsorbent sites which are equivalent, and the surface is homogeneous. The forces of the interaction between adsorbed molecules are negligible. It is seen that the calculated values are listed in Table 1. From Table 1, the experimental data for adsorbent well fit with the Langmuir model and it is realized that calculated $q_{max}$ value for nanoparticles shows close approximation to the experimental values.

$K_L$ in the Langmuir model is a constant attributed to the affinity between the adsorbate and adsorbent [6]. A dimensionless constant called the separation factor ($K_R$) can be used for indicating the type of adsorption using the Langmuir constant $K_L$ as follows:

$$K_R = 1/\left(1 + K_L \cdot C_0\right) \tag{4}$$

$K_R$ value implies the type of adsorption as: $K_R = 0$ irreversible adsorption, $0 < K_R < 1$ favorable adsorption, $K_R = 1$ linear adsorption, and $K_R > 1$ unfavorable adsorption. $K_R$ values gained from the experiment results are between zero and one, showing that the adsorption is favorable.

The re-arranged Freundlich equation can be expressed by Eq. 5:

$$\log q_e = \log K_F + \frac{1}{n} \log C_e \tag{5}$$

where $K_F$ and $n$ are the adsorption capacity and the heterogeneity factor, respectively. If the value of $1/n$ is higher ($1/n > 1$), the adsorption is a more favorable physical process. These are called Freundlich constants characteristic of the system.

The Freundlich isotherm is confined to the formation of the multilayer coverage, and it assumes that adsorption occurs on heterogeneous surface of adsorbent as well as multilayer sorption.

The Freundlich equation has been used to describe sorption of MGB from solution onto nanoparticles. Hence, Eq. 5 is used to calculate the constants which are shown in Table 1. In the Freundlich isotherm, the correlation coefficient for this isotherm plot is 0.91. It can be seen that regression coefficient obtained from the Freundlich

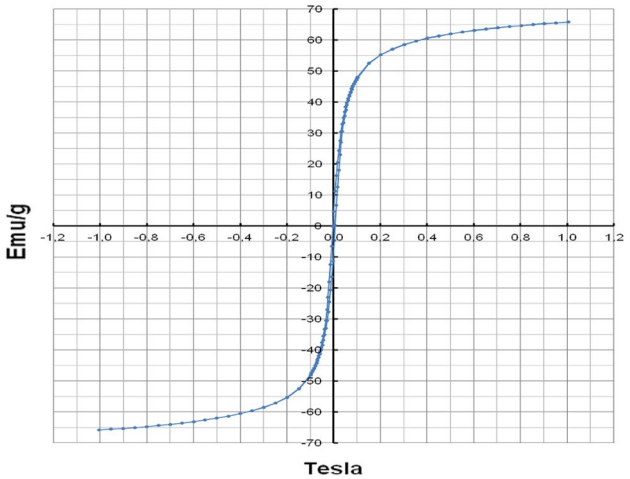


**Fig. 5** VSM analysis of $Fe_3O_4$ nanoparticles

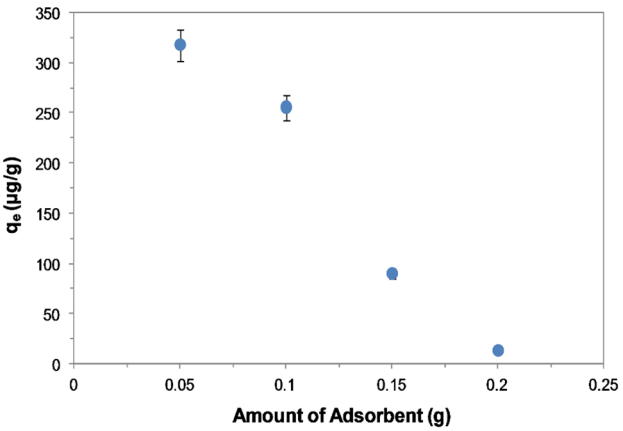


**Fig. 6** Adsorption change depending on the amount of adsorbent

isotherm is lower than the Langmuir isotherm for nanoparticles adsorbent. However, Freundlich model can be used to explain dye adsorption isotherm on nanoparticles at temperatures other than room temperature.

The Temkin isotherm equation estimates that there appears a decrease in the heat of adsorption of all the molecules in layer linearly with coverage because of adsorbent–adsorbate interactions, and that the adsorption is described by a uniform distribution of the bonding energies, up to some maximum binding energy [39]. The Temkin isotherm is given as follows:

$$q_e = RT/b.\ln A + RT/b\ \ln C_e \quad (6)$$

where $A$ is the equilibrium binding constant (L/g), coincident with the maximum binding energy, and constant $b$ is related to the heat of adsorption (J/mol), T is the absolute temperature (K), and $R$ is the universal gas constant (8.314 J/mol K). A plot of $q_e$ versus ln $C_e$ allows the determination of the isotherm constants $b$ and $A$ from the slope and intercept of the straight line plot.

The 3 isotherm model parameters along with the regression coefficients are given in Table 1. The data belonging to the 3 isotherm models showed that the linearity of the Langmuir isotherm models ($R^2 = 0.99$) was higher than that of the other isotherm models according to the room-temperature data (Table 1). This shows that the sorption of MBG on nanoparticles is more of monolayer sorption. According to the other two temperature data, the linearity of Freundlich isotherm model was higher than that of the other isotherm models.

## Adsorption kinetics

Adsorption kinetics of MGB adsorbed onto $Fe_3O_4$ nanoparticles was examined. All experimental studies were carried out in batch system at room temperature. At the end of a given time, $t$, amount of adsorbed MGB per gram of $Fe_3O_4$ nanoparticles, $q_t$, was calculated according to Eq. 1. Graph generated from the obtained data is shown in Fig. 9.

Figure 9 shows the changes in the amounts of the MBG adsorbed over time ($q_t$) calculated using Eq. 1. As can be seen, adsorption of MBG by nanoparticles is fast for the first 10 min and slows down until 30th min, and the equilibrium is reached after 80–100 min. Therefore, optimum removal time for MBG was determined to be 100 min.

Three kinetic models which are Lagergren pseudo-first-order, second-order and intra-particle diffusion models were tested to explain the adsorption kinetics, and the rate constants of MBG on nanoparticles were calculated. Adsorption data were evaluated according to the linearized form of Lagergren pseudo-first-order reaction kinetic formula given by Eq. 7:

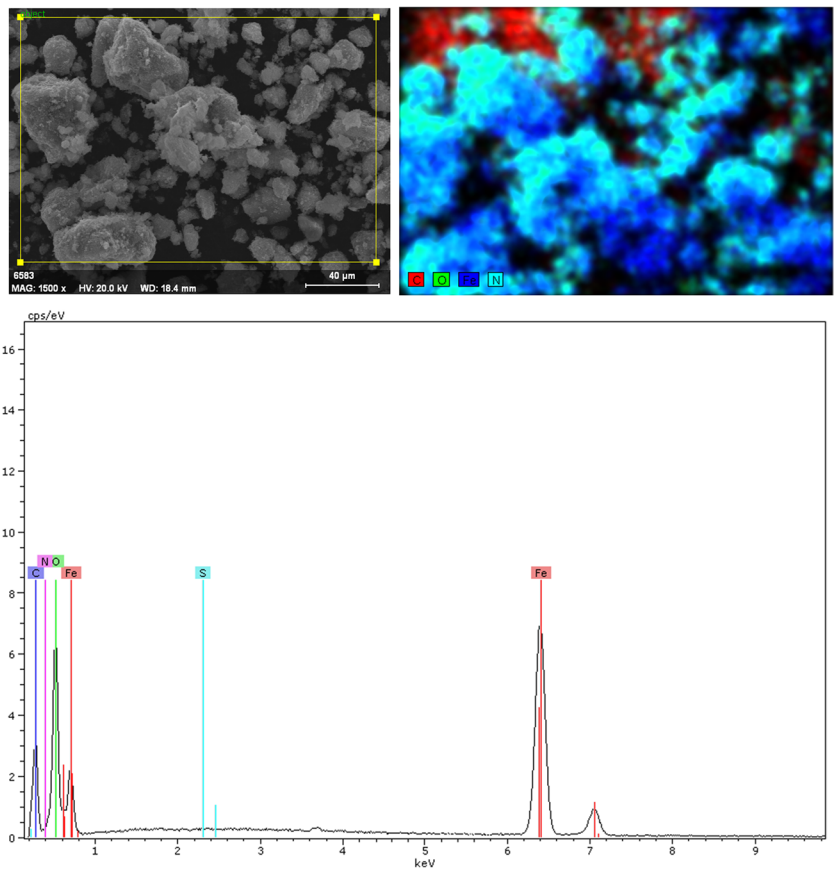


**Fig. 7** SEM–EDS images of MBG adsorbed $Fe_3O_4$ particles

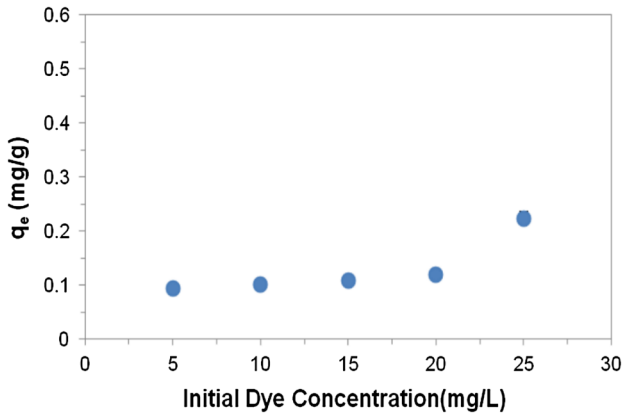


**Fig. 8** The effect of MBG initial concentration on the adsorption capacity

$$\log\left(q_e - q_t\right) = \log\, q_e - \frac{k_1}{2.303}t \tag{7}$$

where $q_e$ and $q_t$ are the amounts of adsorbed dye (mg/g) at equilibrium and at time $t$ (min), respectively, and $k_1$ is the rate constant of the pseudo-first-order reaction ($min^{-1}$). $C_1$ is the integration constant in Eq. 6. The plot of log $(q_e - q_t)$ against t should give the $k_1$ and $q_e$ values from the slope and intercept of the plot, respectively.

The pseudo-second-order kinetic model is given by Eq. 8:

$$\frac{t}{q_t} = \frac{1}{k_2\, q_e^2} + \frac{t}{q_e} \tag{8}$$

where $k_2$ is the rate constant of the pseudo-second-order reaction (mg $g^{-1}$ $min^{-1}$). The plot of $t/q_t$ versus $t$ should give the $k_2$ and $q_e$ values from the slope and intercept of the plot, respectively. Graph of the pseudo-second-order kinetic model is shown in Fig. 10.

The kinetic parameters obtained from the plots in Fig. 10 are given in Table 2. It is seen from Table 2 that the second-order kinetics is in good agreement with data and the second-order kinetics shows closer approximation to the experimental data for $q_e$. Moreover, the correlation coefficient of the second-order reaction kinetics is higher than that of the first-order reaction kinetics. Rate constants are calculated from the slopes of the curves (Table 2). Compared with the experimental equilibrium adsorption value, $q_e$, the second-order kinetics produces a much closer value and it seems possible to suggest that the adsorption of MBG onto nanoparticles follows a second-order-type reaction kinetics. But the pseudo-second-order kinetics model could not identify the diffusion mechanism.

In presenting the adsorption mechanism, three steps have to be taken into consideration. The first one is the film or surface diffusion. Dye moves through the solution to the exterior surface of $Fe_3O_4$ adsorbent. The second one is the intra-particle or pore diffusion. MGB moves within the particle agglomerated. The final one is the adsorption on the interior sites of adsorbents, which occurs very fast. Therefore, it is ignored for describing the overall rate of adsorption process. During this process, MGB dye is adsorbed at sites on the interior surface of $Fe_3O_4$ particle agglomerated. In order to clarify adsorption mechanism, Weber and Morris intra-particle diffusion model has often been used to determine the rate-limiting step [41]. General representation of the kinetics model is expressed as follows:

$$q_t = k_{id} \cdot t^{0.5} + C_i \tag{9}$$

where $k_{id}$ is the intra-particle diffusion rate constant (mg $g^{-1}$ $min^{-0.5}$) and $C_i$ is the intercept. The plot of $q_t$ versus $t^{0.5}$ should give the $k_{id}$ and $C_i$ values from the slope and intercept of the plot, respectively. The value of $C$ also clears up information about the thickness of the boundary layer.

In agreement with this model, on the condition that the plot does not go through the origin, intra-particle diffusion is not the only rate-limiting step. In addition to first activity, the other kinetic models may control the rate of adsorption.

The plot of $q_t$ versus $t^{0.5}$ may display a multi-linearity showing two or more steps for adsorption process [7, 46] (Fig. 11). This plot proposes that adsorption of dye on nanoparticles took place in three phases. The initial steeper section exemplifies the surface or film diffusion, the second linear section serves as a gradual adsorption stage in which intra-particle or pore diffusion is rate-limiting, and the third section is the final equilibrium stage. If the plot did not go through the origin, intra-particle diffusion was not the only rate-controlling step. Thus, there were three processes controlling the adsorption rate, but only one was the rate-limiting process in any particular time range. The intra-particle diffusion rate constants $k_i$ and $C$ were adjusted from the slope of the second linear section. It was observed from the plot that the straight lines did not pass through the

**Table 1** Parameters of adsorption isotherm of MBG on $Fe_3O_4$

| Temperature (K) | Langmuir isotherm | | | Freundlich isotherm | | | Temkin isotherm | | |
|---|---|---|---|---|---|---|---|---|---|
| | $q_{max}$ | $K_L$ | $R^2$ | $K_F$ | $n$ | $R^2$ | $b$ | $A$ | $R^2$ |
| 298 | 0.13 | 0.48 | 0.99 | 0.075 | 6.6 | 0.91 | $1.6\times10^5$ | 4.6 | 0.92 |
| 308 | 0.28 | 0.032 | 0.71 | 0.012 | 1.3 | 0.97 | $5.2\times10^4$ | 0.43 | 0.92 |
| 318 | 2.1 | 0.045 | 0.94 | 0.019 | 0.91 | 1.0 | $1.2\times10^4$ | 0.34 | 0.95 |

origin, and this further notes that the intra-particle diffusion is not the only rate-controlling step. Experimental results show similarities to Doğan et al.'s work [2, 3, 9, 33].

### The effect of pH on dye adsorption

The experiments were performed with 25 mg/L dye solution that has 5, 7, 9 pH value to examine the effect of pH on the adsorption. The gained data are given in Fig. 12 as a graph.

As shown in Fig. 12, as the pH of solution increases so will the adsorption of dye. When the pH of solution is 5, the adsorption capacity has reached up to about 0.10 mg/g. While the pH of solution is 9, the amount of the adsorption capacity has gone up to about 1.0 mg/g. This is because the adsorbent material, iron oxide nanoparticles, is positively charged in the acidic pH and is negatively charged in the basic pH [8]. While the pH of the solution starts to increase, the negative charge density on the adsorbent surface starts to increase. Thus, the cation of the dye goes into interaction more easily with the negatively charged adsorbent surface due to electrostatic interaction [3, 9]. However, the negative charge impact formed by unpaired electrons of nitrogen that exists in the acidic pH of the dye molecules influences $H^+$ ions electrostatically present in the environment, causing positively charged areas in the dye. In acidic environments, since there are the negatively charged ends in the dye molecule as well as the positively charged areas, it leads to generation of the repulsive forces between these areas and the positively charged adsorbent material. Thus, a slight decrease in the amount of adsorption is seen. During the water treatment processes, acidic water is generally undesirable and in many of the processes, neutralization is implemented to ensure the discharge criteria. When the studies are evaluated in this scope, it is a desirable situation for the facilities to have more productivity of dye removal at the water treatment plants.

### The effect of temperature on dye adsorption

The effect of the temperature on MBG adsorption was studied in 3 different temperatures, and the gained data are provided in Fig. 13 as a graph.

When Fig. 13 is examined in general, it appears that as the ambient temperature increases, the adsorption of MBG increases. As the adsorption increases with the increasing temperature, it can be interpreted as an increase in the rate of the dye molecules. The ΔS°, ΔH° and ΔG° values calculated from the temperature data using related equations [1] are 156 J/K, 53.9 kJ/mol and 7.38 kJ/mol, respectively. This situation has shown that the dye adsorption takes place on the $Fe_3O_4$ particles in the endothermic form [9, 32]. It is known that some of the processes performed in the printing and dyeing units of textile industry are carried out at elevated temperatures. In such cases, the waste water containing dyes are sent to the treatment plant at high temperatures. Given the fact that adsorption increases at 318 K temperature, it is possible to conclude with the $Fe_3O_4$ nanoparticles in textile industry, high adsorption efficiency can be achieved.

## Conclusion

$Fe_3O_4$ was synthesized by using co-precipitation method and used as adsorbent for the removal of MBG from aqueous solutions. It was determined from the XRD pattern that the synthesized particles are in compliance with iron oxide ($Fe_3O_4$). It was seen in the SEM and TEM images that the particles were agglomerated and one particle was in the size of 10–15 nm. The average crystallite size of magnetite found as 13.2 nm has been calculated by using Scherrer equation and the data obtained from the XRD analysis. After VSM analysis, it was determined that the particles are superparamagnetic and the saturation magnetization

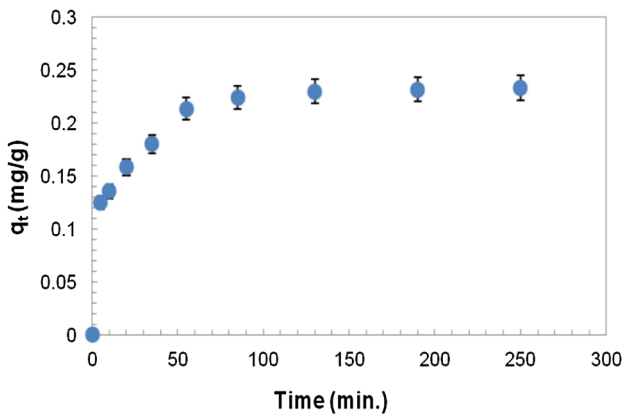


**Fig. 9** Adsorption kinetics of $Fe_3O_4$ nanoparticles

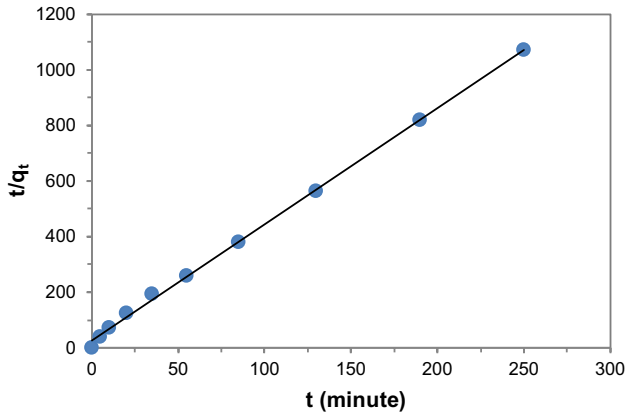


**Fig. 10** Pseudo-second-order kinetic model for adsorption of MBG

**Table 2** Parameters of pseudo-first and second-order kinetic model for MBG adsorption on $Fe_3O_4$

| Adsorbent | $q_e$ (mg/g) (experimental) | First-order | | | Second-order | | |
|---|---|---|---|---|---|---|---|
| | | $q_e$ (mg/g) (calculated) | $k_1$ ($min^{-1}$) | $R^2$ | $q_e$ (mg/g) (calculated) | $k_2$ (g $mg^{-1}$ $min^{-1}$) | $R^2$ |
| $Fe_3O_4$ | 0.23 | 0.13 | $2.7\times10^{-2}$ | 0.96 | 0.24 | $6.5\times10^{-1}$ | 1.0 |

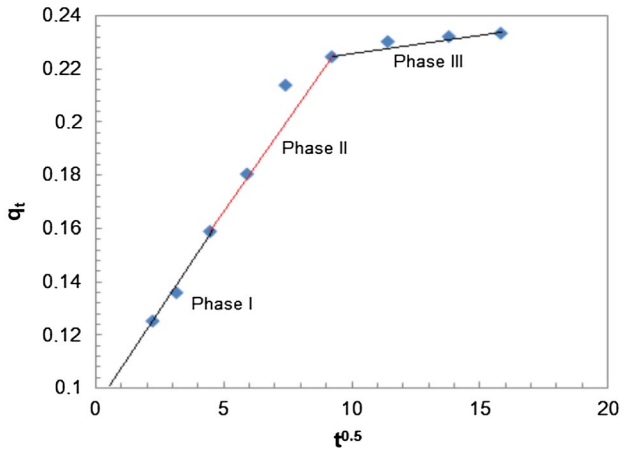


**Fig. 11** Intra-particle diffusion plot

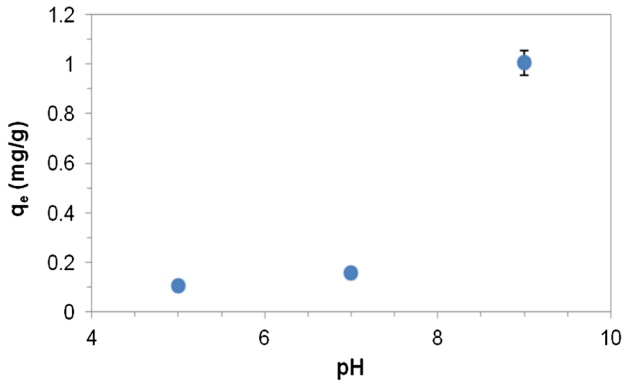


**Fig. 12** The effect of pH on the adsorption of MBG

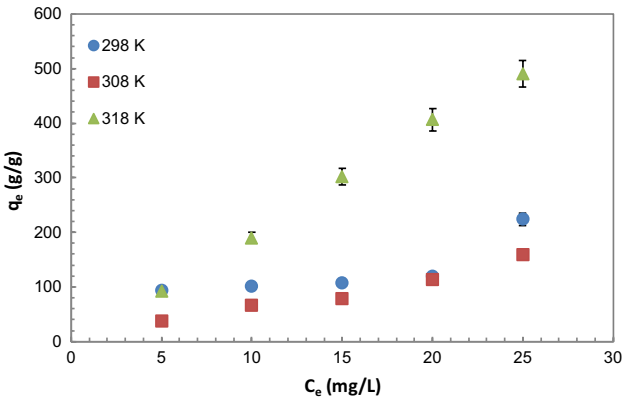


**Fig. 13** The effect of the temperature on MBG adsorption

(Ms) value is 66.50 emu/g. In adsorption studies, the effects of adsorbent dosage, contact time, initial MBG concentrations, pH and temperature on the adsorption were investigated. After the adsorption process, N atoms have also been detected as well as C atoms on the $Fe_3O_4$ surface through EDS analysis. When test results were compared, it can be said that the capacity of dye removal of $Fe_3O_4$ particles goes up with the increased dye concentration, pH and temperature. Because of the increase in the interaction of negatively charged $Fe_3O_4$ particles with the positively charged dye when the pH value of environment rises up, there occurs an increase in the adsorption. As driving force is concentration gradient in the increasing dye concentration, an increase was observed in the adsorption. It was understood in the examination of the adsorption isotherm that it fits the Langmuir isotherm at room temperature that means that the adsorption occurred in a monolayer form. However, it was understood that the adsorption fits the Freundlich isotherm with the increase in temperature, that is the adsorption occurred in a multilayer form. The results of adsorption kinetics and thermodynamic data have shown that adsorption process has pseudo-second-order kinetics and endothermic form. This study proves that $Fe_3O_4$ is efficiently usable in the textile industry where hot water washing is carried out at the basic pH values of waste water. Behavior of the synthesized $Fe_3O_4$ against the dye molecules is very useful, and it has a potential to be used as an adsorbent for the textile waste water.

**Acknowledgements** This study was supported by TUBITAK (1139B411500163). The authors would like to thank Mahfus Doğan, Ozan Aslan and Ömer Özbek for their contributions. The authors would like to thank METU Central Laboratory and TUAM at Afyon Kocatepe University for all characterization analyses and to thank Bilimteks Company.

## References

1. Akın D, Yakar A, Gündüz U (2015) Synthesis of magnetic $Fe_3O_4$-chitosan nanoparticles by ionic gelation and their dye removal ability. Water Environ Res 87:425–436
2. Aljeboree AM, Radi N, Ahmed Z, ve Alkaim AF (2014) The use of sawdust as by product adsorbent of organic pollutant

from wastewater: adsorption of maxilon blue dye. Int J Chem Sci 12(4):1239–1252
3. Alkaim AF, Sadik Z, Mahdi DK, Alshrefi SM, Al-Sammarraie AM, Alamgir FM, Singh PM, Aljeboree AM (2015) Preparation, structure and adsorption properties of synthesized multiwall carbon nanotubes for highly effective removal of maxilon blue dye. Korean J Chem Eng 32:2456–2462
4. Banat F, Al-Asheh S, Al-Makhedmeh L (2003) Evaluation of the use of raw and activated date pits as potential adsorbents for dye containing waters. Process Biochem 39:193–202
5. Baumgartner J, Bertinetti L, Widdrat M, Hirt AM, Faivre D (2013) Formation of magnetite nanoparticles at low temperature: from superparamagnetic to stable single domain particles. PLoS ONE 8(3):e57070. https://doi.org/10.1371/journal.pone.0057070
6. Behnajady MA, Yavari S, Modirshahla N (2014) Investigation on adsorption capacity of $TiO_2$-P25 nanoparticles in the removal of a mono-azo dye from aqueous solution: a comprehensive isotherm analysis. Chem Ind Chem 20:97–107
7. Boparai HK, Joseph M, O'Carroll DM (2011) Kinetics and thermodynamics of cadmium ion removal by adsorption onto nano zerovalent iron particles. J Hazard Mater 186:458–465
8. Broomberg J, Gelinas S, Finch JA, Xu Z (1999) Review of magnetic carrier technologies for metal ion removal. Magn Electr Sep 9:169–188
9. Doğan M, Alkan M, Demirbas Ö, Özdemir Y, Özmetin C (2006) Adsorption kinetics of maxilon blue GRL onto sepiolite from aqueous solutions. Chem Eng J 124:89–101
10. Dönmez G, Aksu Z (2002) Removal of chromium(VI) from saline wastewaters by Dunaliella species. Process Biochem 38:751–762
11. Freundlich H (1926) Colloid and capillary chemistry. Methuen, London, p 39
12. Gao H, Zhao S, Cheng X, Wang X, Zheng L (2013) Removal of anionic azo dyes from aqueous solution using magnetic polymer multi-wall carbon nanotube nanocomposite as adsorbent. Chem Eng J 223:84–90
13. Ge F, Ye H, Li MM, Zhao BX (2012) Efficient removal of cationic dyes from aqueous solution by polymer-modified magnetic nanoparticles. Chem Eng J 198–199:11–17
14. Ghandoor HE, Zidan HM, Khalil MMH, Ismail MIM (2012) Synthesis and some physical properties of magnetite ($Fe_3O_4$) nanoparticles. Int J Electrochem Sci 7:5734–5745
15. Gnanaprakash G, Mahadevan S, Jayakumar T, Kalyanasundaram P, Philip J, Raj B (2007) Effect of initial pH and temperature of iron salt solutions on formation of magnetite nanoparticles. Mater Chem Phys 103:168–175
16. Gnanaprakash G, Philip J, Jayakumar T, Raj B (2007) Effect of digestion time and alkali addition rate on physical properties of magnetite nanoparticles. J Phys Chem 111:7978–7986
17. Hariani PL, Faizal M, Marsi R, Setiabudidaya D (2013) Synthesis and properties of $Fe_3O_4$ nanoparticles by co-precipitation method to removal procion dye. IJESD 4:336–340
18. Ho YS, Chiang TH, Hsuesh YM (2005) Removal of basic dye from aqueous solution using tree fern as a biosorbent. Process Biochem 40:119–124
19. Huang YH, Hsueh CL, Huang CP, Su LC, Chen CY (2007) Adsorption thermodynamic and kinetic studies of Pb(II) removal from water onto a versatile $Al_2O_3$-supported iron oxide. Sep Purif Technol 55:23–29
20. Jadhav SA, Patil SV (2014) Facile synthesis of magnetic iron oxide nanoparticles and their characterization. Front Mater Sci 8:193–198
21. Juang RS, Wu FC, Tseng RL (1997) The ability of activated clay for the adsorption of dyes from aqueous solutions. Environ Technol 18:525–531
22. Khosravi M, Azizian S (2014) Adsorption of anionic dyes from aqueous solution by iron oxide nanospheres. J Ind Eng Chem 20:2561–2567
23. Kim DK, Zhang Y, Voit W, Rao KV, Muhammed M (2001) Synthesis and characterization of surfactant-coated superparamagnetic monodispersed iron oxide nanoparticles. J Magn Magn Mater 225:30–36
24. Langmuir I (1918) The adsorption of gases on plane surfaces of glass, mica and platinum. J Am Chem Soc 40:1361–1403
25. Li L, Duan H, Wang X, Luo C (2015) Fabrication of novel magnetic nanocomposite with a number of adsorption sites for the removal of dye. Int J Biol Macromol 78:17–22
26. Lillo-Rodenas MA, Marco-Lozar JP, Cazorla-Amoros D, Linares-Solano A (2007) Activated carbons prepared by pyrolysis of mixtures of carbon precursor/alkaline hydroxide. J Anal Appl Pyrol 80:166–174
27. Lin CC, Lin YS, Ho YM (2016) Adsorption of Reactive Red 2 from aqueous solutions using $Fe_3O_4$ nanoparticles prepared by co-precipitation in a rotating packed bed. J Alloy Compd 666:153–158
28. Madrakian T, Afkhami A, Kashani HM, Ahmadi M (2013) Adsorption of some cationic and anionic dyes on magnetite nanoparticles-modified activated carbon from aqueous solutions: equilibrium and kinetics study. J Iran Chem Soc 10:481–489
29. Madrakian T, Afkhami A, Zolfigol MA, Ahmadi M, Koukabi N (2012) Application of modified silica coated magnetite nanoparticles for removal of iodine from water samples. Nano Micro Lett 4:57–63
30. Mascolo MC, Pei Y, Ring TA (2013) Room temperature co-precipitation synthesis of magnetite nanoparticles in a large pH window with different bases. Materials 6:5549–5567
31. Monshi A, Foroughi MR, Monshi MR (2012) Modified Scherrer equation to estimate more accurately nano-crystallite size using XRD. WJNSE 2:154–160
32. Namasivayam C, Radhika R, Suba S (2001) Uptake of dyes by a promising locally available agricultural solid waste: coir pith. Waste Manag 21:381–387
33. Nas MS (2019) The investigation of thermodynamics parameters and adsorption kinetic of the maxilon blue 5G dye on Turkey green clay. Iğdır Üniv Fen Bilim Enst Derg 9:749–758
34. Shao H, Yoon TJ, Liong M, Weissleder R, Lee H (2010) Magnetic nanoparticles for biomedical NMR-based diagnostics. Beilstein J Nanotechnol 1:142–154
35. Shen L, Qiao Y, Guon Y, Meng S, Yang G (2014) Facile co-precipitation synthesis of shape-controlled magnetite nanoparticles. Ceram Int 40:1519–1524
36. Sivashankar R, Sathya AB, Vasantharaj K, Sivasubramanian V (2014) Magnetic composite an environmental super adsorbent for dye sequestration. Environ Nanotechnol Monit Manag 1–2:36–49
37. Song W, Gao B, Xu X, Xing L, Han S, Duan P, Song W, Jia R (2016) Adsorption–desorption behavior of magnetic amine/$Fe_3O_4$ functionalized biopolymer resin towards anionic dyes from wastewater. Bioresour Technol. https://doi.org/10.1016/j.biortech.2016.01.078
38. Stephen Inbaraja B, Chen BH (2011) Dye adsorption characteristics of magnetite nanoparticles coated with a biopolymer poly(γ-glutamic acid). Bioresour Technol 102:8868–8876
39. Temkin MJ, Pyzhev V (1940) Kinetics of ammonia synthesis on promoted iron catalysts. Acta Physicochitnica URSS 12:217–222
40. Wang B, Wei Q, Qu S (2013) Synthesis and characterization of uniform and crystalline magnetite nanoparticles via oxidation-precipitation and modified co-precipitation methods. Int J Electrochem Sci 8:3786–3793
41. Weber WJ, Smith EH (1987) Simulation and design models for adsorption processes. Environ Sci Technol 21:1040–1050

42. Yakar A, Tansık G, Keskin T, Gündüz U (2013) Tailoring the magnetic behavior of polymeric particles for bioapplications. J Polym Eng 33:265–274
43. Yao T, Guo S, Zeng C, Wang C, Zhang L (2015) Investigation on efficient adsorption of cationic dyes on porous magnetic polyacrylamide microspheres. J Hazard Mater 292:90–97
44. Yuan X, Zhuo SP, Xing W, Cui HY, Dai XD, Liu XM, Yan ZF (2007) Aqueous dye adsorption on ordered mesoporous carbons. J Colloid Interface Sci 310:83–89
45. Zhao S, Asuha S (2010) One-pot synthesis of magnetite nanopowder and their magneticproperties. Powder Technol 197:295–297
46. Zheng H, Liu D, Zheng Y, Liang S, Liu Z (2009) Sorption isotherm and kinetic modeling of aniline on Cr-bentonite. J Hazard Mater 167:141–147
47. Zhou Z, Lin S, Yue T, Lee TC (2014) Adsorption of food dyes from aqueous solution by glutaraldehyde cross-linked magnetic chitosan nanoparticles. J Food Eng 126:133–141